buildings

MDPI

Article

Field Experimental Study on the Uplift and Lateral Capacity of Deep Helical Anchors and Grouped Helical Anchors in Clays

Chi Yuan [1], Dongxue Hao [2,*], Shijun Ding [3] and Mintao Ding [3]

[1] College of Architecture and Civil Engineering, Beijing University of Technology, Beijing 110124, China; yuanc@emails.bjut.edu.cn
[2] Key Laboratory of Electric Power Infrastructure Safety Assessment and Disaster Prevention of Jilin Province, Northeast Electric Power University, Jilin 132012, China
[3] China Electric Power Research Institute, Beijing 100055, China; dingsj@epri.sgcc.com.cn (S.D.); dingmintao@epri.sgcc.com.cn (M.D.)
* Correspondence: 20102291@neepu.edu.cn; Tel.: +86-432-6480-6481

Abstract: This research aims to investigate the bearing capability of deep helical anchors and grouped helical anchors under uplift or lateral loads using field experiments. Grouped helical anchors may serve as a viable alternative to traditional deep foundations, offering increased resistance against uplift and lateral forces. The study of group effect primarily focuses on vertically installed helical anchors, with few data available on various configurations of grouped helical anchors. This research includes a total of 12 single-helix anchors, 4 double-helix anchors, and 4 grouped helical anchors, with anchor plate diameters of 400 mm and maximum embedment depths of 7.4 m. There are two configurations of grouped helical anchors, each with different platforms. This article studies the effect of some factors, including the embedment depth, the number of anchor plates, the spacing between anchor shafts, the selection of failure criteria, and the group effect. The primary findings indicate that adding the anchor plates to single-helix anchors without extending the shaft length does not increase uplift or lateral capacity. In this soil condition, the group efficiency of double-helix anchors is higher than 1. By comparing the group efficiency and economy of the G1 and G2 grouped helical anchors, it is highly recommended to use the G2 configuration. The data obtained from this work may also serve as a valuable tool for validating numerical models used to analyze interactions among grouped helical anchors.

Keywords: grouped helical anchor; group efficiency; uplift capacity; lateral capacity

Citation: Yuan, C.; Hao, D.; Ding, S.; Ding, M. Field Experimental Study on the Uplift and Lateral Capacity of Deep Helical Anchors and Grouped Helical Anchors in Clays. *Buildings* **2024**, *14*, 662. https://doi.org/10.3390/buildings14030662

Academic Editors: Junyoung Ko, Joonkyu Lee and Jaehyun Kim

Received: 26 January 2024
Revised: 19 February 2024
Accepted: 28 February 2024
Published: 1 March 2024

1. Introduction

A helical anchor, also known as a helical pile, consists of an anchor head, anchor plate, anchor shaft, and connection, which are joined together by either welding or prefabrication. Based on the number of anchor shafts, it may be categorized into single-helix anchors and grouped helical anchors. The helical anchor differs from the standard pile foundation in using torque to screw the anchor into the earth, enabling it to withstand more pressure, uplift, and lateral load [1–5]. In contrast to the conventional pile foundation, the helical anchor foundation has the advantages of quick and easy installation, little noise during construction, rapid use after installation, and the ability to be reused several times [6–13]. The helical anchor is used as the foundation for many structures such as coastal wharves, wind power generators, overhead transmission lines, natural gas platforms, and high-rise skyscrapers due to its numerous benefits [12,14–17]. In particular, helical anchors have significant capacity and have recently been proposed by many researchers for offshore applications [18–21]. For low upper loads, one may use either a big single-helix anchor or a tiny grouped helical anchor. As the load carried by the superstructure increases, the design parameters of the grouped helical anchor, such as embedment depth, anchor plate diameter, anchor plate quantity, and foundation shape, must be adjusted correspondingly. Machine learning, artificial intelligence, and artificial neural network (ANN) algorithms are expected to develop a more accurate and reliable tool for determining the load-bearing capacity (LBC) of helical anchors [22–25]. Such models can be specifically established to provide quick and precise predictions of the LBC under various loading conditions, including axial, lateral, and inclined loads [26,27].

A group of researchers has investigated the behavior of helical anchors in cohesionless soil [28–34] as well as in cohesive soil [35–38] using numerical, experimental, and field tests. Two failure mechanisms, the individual pile failure mechanism, and the block failure mechanism, which is dependent on the spacing between the anchors, are available when the grouped helical anchor is loaded vertically. The group effect will gradually diminish as the anchor spacing increases [39,40]. In a study conducted by Radhakrishna, a single vertical uplift test was conducted on a group of triple-helix anchors arranged in a 2×2 configuration. The anchors were installed in stiff fissured clay. The results showed that spacing the anchors at approximately three times the diameter of the largest helix did not lead to a significant decrease in the uplift capacity of each individual anchor [41]. The characteristics of grouped helical anchors under lateral static [21,35,42–45] and dynamic loads [46–50] have been studied. In a study conducted by Venkatesan Vignesh, the uplift and lateral behavior of group piles installed in soft clay soil was studied using a finite element and 1 g model experiment. The findings showed that the group efficiency is significantly influenced by the number of anchors, center-to-center anchor spacing, and the failure criteria assumed to interpret test data [21]. However, the majority of the studied grouped helical anchors consist of vertical single-helix anchors, and there is a scarcity of studies on other configurations of grouped helical anchors.

The purpose of this research was to examine the bearing characteristics of deep helical anchors. Two configurations of grouped helical anchors were designed in accordance with engineering requirements, and helical anchors were subjected to either uplift or lateral loads. Furthermore, we augmented the current data on the impacts of grouped helical anchors by conducting a field study. The following sections of this paper include a comprehensive account of the test site, design, methods, results, and discussion.

2. Test Site and Design

2.1. Test Site

The test site was located at Yuncheng, Shanxi, China. The area is in the Quaternary late Pleistocene alluvial layer, and the lithology is mainly clay, belonging to the accumulation terrain, as shown in Figure 1. Through field drilling combined with laboratory test results, it was determined that the soil texture of the stratum is relatively uniform. It is clay, brown, slightly wet, and slightly dense from the surface to a depth of 13.5 m. This soil layer contains white mycelia and calcareous nodules which are without a gloss reaction and have low dry strength, low toughness, and a moderate shaking response. According to geological survey and excavation results, no groundwater was found within 15.0 m. The physical and mechanical parameters of the soil layer in the site were obtained through indoor geotechnical tests, as shown in Table 1. Using the modified Cam Clay yield criterion, we estimated the OCR to be between 5 and 10 based on a comparison of the prior consolidation pressure with the current pressure [51–54].

Table 1. Physico-mechanical property indices of soil layers.

Soil Type	Water Content (%)	Density (g/cm^3)	Gravity	Void Ratio (%)	Compression Modulus (MPa)	Liquid Limit (%)	Plastic Limit (%)	Internal Friction Angle (°)	Cohesion (kPa)
Clay	12.4	1.48	2.7	1.055	7.59	23.6	14.9	27.1	15.9

Figure 1. Test site.

2.2. Test Design

A total of 20 field load tests were conducted using round-shaft helical anchors, including 12 single-helix anchor tests, 4 double-helix anchor tests, and 4 grouped helical anchor tests. The field load test scheme is shown in Table 2; in the test numbers, S represents a single helical anchor, D represents a double-helix anchor, and G represents a grouped helical anchor.

Table 2. Field load test scheme.

Test Number	Direction of Test Load	Embedment Depth H (m)	Anchor Plate Number n	Anchor Plate Spacing S (m)	Inclination Angle α (°)
S1	Uplift	6.0	1	0	0
S2	Uplift	6.0	2	1.2	0
S3	Uplift	6.0	3	1.2	0
S4	Uplift	6.0	4	1.2	0
S5	Uplift	6.0	4	1.2	12°
S6	Uplift	6.0	4	1.2	17°
S7	Uplift	7.4	1	0	0
S8	Lateral	6.0	1	1.2	0
S9	Lateral	6.0	2	1.2	0
S10	Lateral	6.0	3	1.2	0
S11	Lateral	6.0	4	1.2	0
S12	Uplift	4.8	1	0	0
D1	Uplift	6.0	1	0	0
D2	Uplift	6.0	1	0	0
D3	Uplift	6.0	4	1.2	0
D4	Uplift	6.0	4	1.2	0
G1-U	Uplift	6.0	4	1.2	0, 7, 7, 10
G1-L	Lateral	6.0	4	1.2	0, 7, 7, 10
G2-U	Uplift	6.0	4	1.2	12, 17, 17
G2-L	Lateral	6.0	4	1.2	12, 17, 17

The helical anchors were made of Q345 steel (Young Modulus and = 210 GPa, yield stress = 345 MPa, and tensile stress = 470~630 MPa). The anchor proportions are based on some of the largest commercially available helical anchors, consisting of 114 mm diameter anchor shafts (d) and a wall thickness of 8 mm. The helix plate diameter (D) is 400 mm with a thickness of 10 mm and a pitch of 100 mm. The number of anchor plates (n) is 1 to 4, and the spacing (S) between anchor plates is 1.2 m. The embedment depth (H) of the helical anchors was 4.8 m to 7.4 m. The partial design drawings of those helical anchors are shown in Figure 2, where Figure 2a is a single-helix anchor, Figure 2b is a grouped helical anchor used in the G1 tests, and Figure 2c is a grouped helical anchor used in the G2 tests. The double-helix anchors consist of two single-helix anchors in which the distance between the shaft of D1 and D3 (l) is 3D and the l of D2 and D4 is 4D. Two types of grouped helical anchors were designed based on the upper load in engineering needs, G1 and G2. G1 consists of a reinforced concrete platform and four single-helix anchors with one inclination angle (α) of 10°, two inclination angles of 7°, and one inclination angle of 0°. G2 consists of a steel platform and three single-helix anchors with two inclination angles of 17° and one inclination angle of 12°.

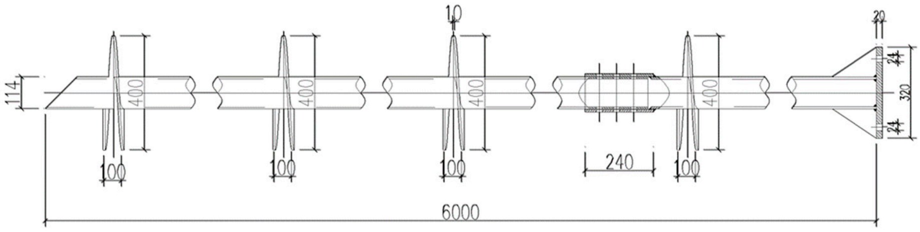

(**a**) Single-helix anchor (S4)

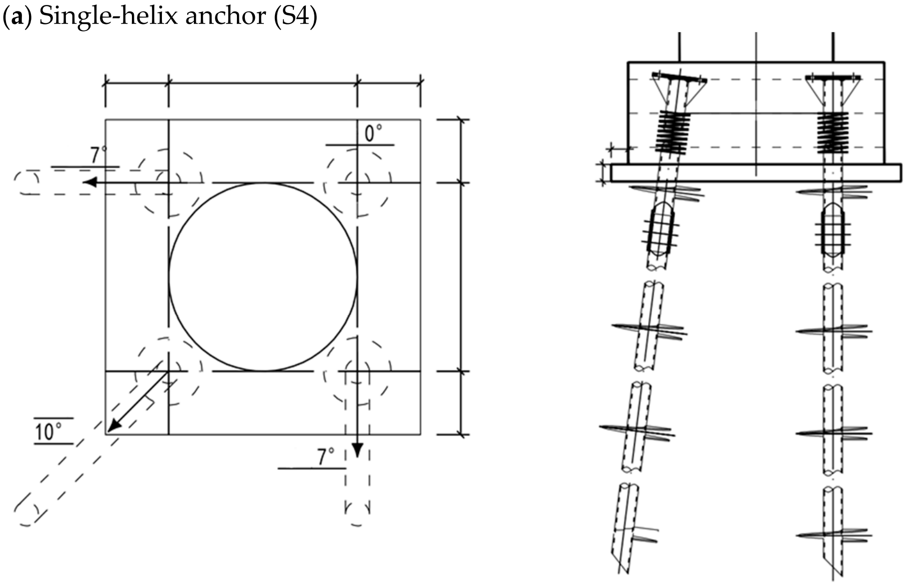

(**b**) Grouped helical anchor (G1)

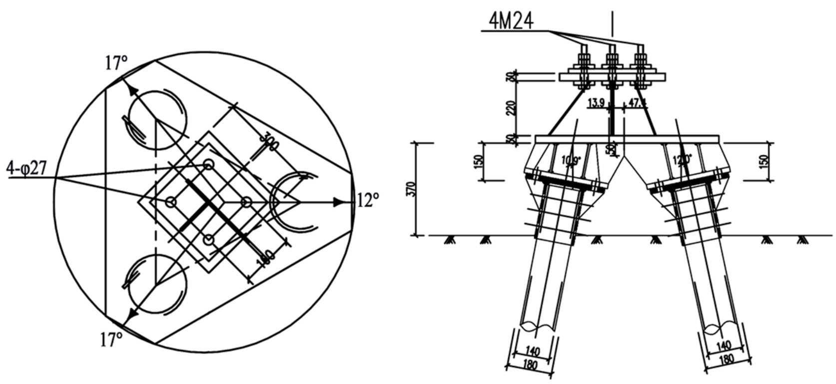

(**c**) Grouped helical anchor (G2)

Figure 2. Design drawing.

The installation process is shown in Figure 3. The rotary drilling driver was used to install the helical anchors, as shown in Figure 3a, and the advancement ratio (AR) was set to 1. An advancement ratio of 1.0 would indicate a "pitch-matched" installation. Firstly, we determined the position and inclination of the helical anchor to be installed. During the installation process, we rotated it at one revolution per minute and then paused the installation for ten revolutions each time in order to re-measure the position and inclination. We ensured that the position error was no greater than 10 mm and the inclination error was no greater than 1°. After installation, all single-helix anchors had a space of 300 mm at the top (in which to apply the load), as shown in Figure 3b. The double-helix anchor was placed with a connector on the top of the anchor, and the weight of the connector was subtracted from the subsequent results, as shown in Figure 3c. The grouped helical anchor used a cast-in-place pile foundation as a reaction pile, as shown in Figure 3d.

(**a**) Construction process

(**b**) Single-helix anchor

Figure 3. *Cont*.


(**c**) Double-helix anchor


(**d**) Grouped helical anchor

Figure 3. Photograph showing a typical load test setup for the helical anchors.

We performed real-time detection of changes in installation torque during installation from the driver hydraulic pressure. The installation torques at different inclinations are shown in Figure 4. It can be observed that the inclination has a small impact on the installation torque. The installation torques associated with various depths were averaged.

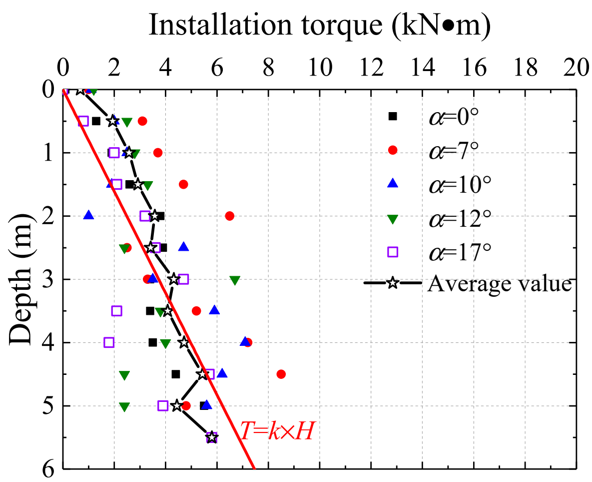

Figure 4. The relationship between installation torque and depth.

According to Figure 4, we calculated the correlation between the installation torque calculated and the depth after linear fitting, as shown in Equation (1).

$$T = k \times H \tag{1}$$

where T is the installation torque, kN·m; k is the slope, equal to 0.8042 kN; and H is the embedment depth, m.

The layout of the in situ test for the helical anchors is shown in Figure 5. The control room is equipped with a load control system and a data acquisition system. Different tests were positioned according to the layout, using the scale in the bottom left as the reference. All tests were conducted by applying a load on the top of the anchor through a hydraulic jack via a transmission device. The hydraulic jack was located on the top of the reaction beam, which was bolted to the reaction pile. The test sequence was to test the single-helix anchor first, followed by the double-helix anchor and the grouped helical anchor. During the test, the single-helix anchor was tested separately to avoid interaction with the others.

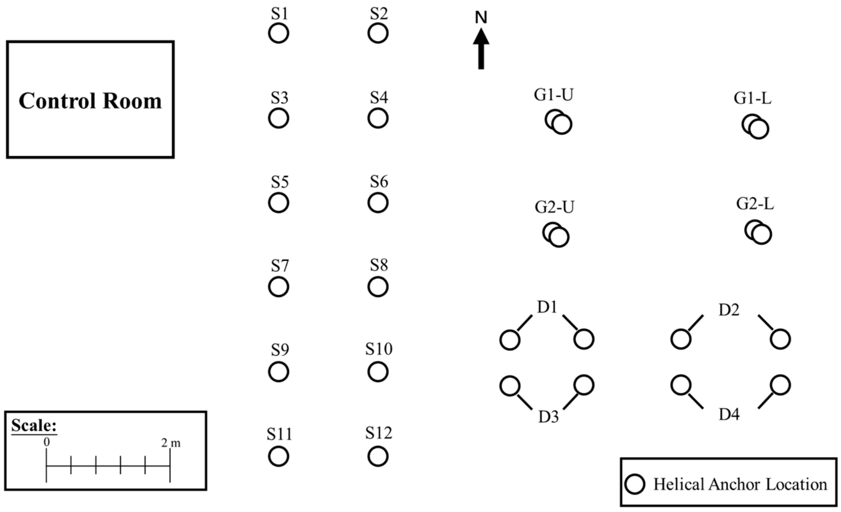

Figure 5. Test site layout showing the locations of helical anchors. **Note:** S represents a single-helix anchor, D represents a double-helix anchor, and G represents a grouped helical anchor.

All pile testing was followed the ASTM "quick test" axial compression load test procedure (D1143/D1143M-07) [35]. The anchors were tested after installation by applying incremental loads; each additional load was 1/8 of the estimated undrained ultimate load capacity and was held for a period of 5 min. The undrained ultimate load capacity of deep helical piles and anchors in clays is generally found using

$$Q_u = s_u N_c A \tag{2}$$

where Q_u is the uplift failure capacity, s_u is the undrained shear strength, N_c is the deep bearing capacity factor (typically taken to be 9.0), and A is the area of the helical plate. The helical anchors were loaded using three types of hydraulic jacks, that is 50 kN, 500 kN, and 1000 kN, and loads were measured with various capacity load cells as needed. Loads were calculated from the hydraulic jack pressure and effective piston area, which gave almost identical results to the load cell measurements. The displacements of helical anchors were also measured with a linear variable displacement transducer or dial gauge fixed to the reaction beam. All instruments were integrated with a data acquisition system and laptop computer. Additionally, the process of unloading used the same method.

3. Results

The load–displacement curves obtained through the site test are shown in Figure 6, where the single-helix anchor under the uplift load is shown in Figure 6a,b, the single-helix anchor under the lateral load is shown in Figure 6c, the double-helix anchor under the uplift load is shown in Figure 6d, and the grouped helical anchor under the uplift and lateral load is shown in Figure 6e,f. Note that the load was adjusted to remove both the weight of the anchor and connector and the initial slack in the system as the load was applied.

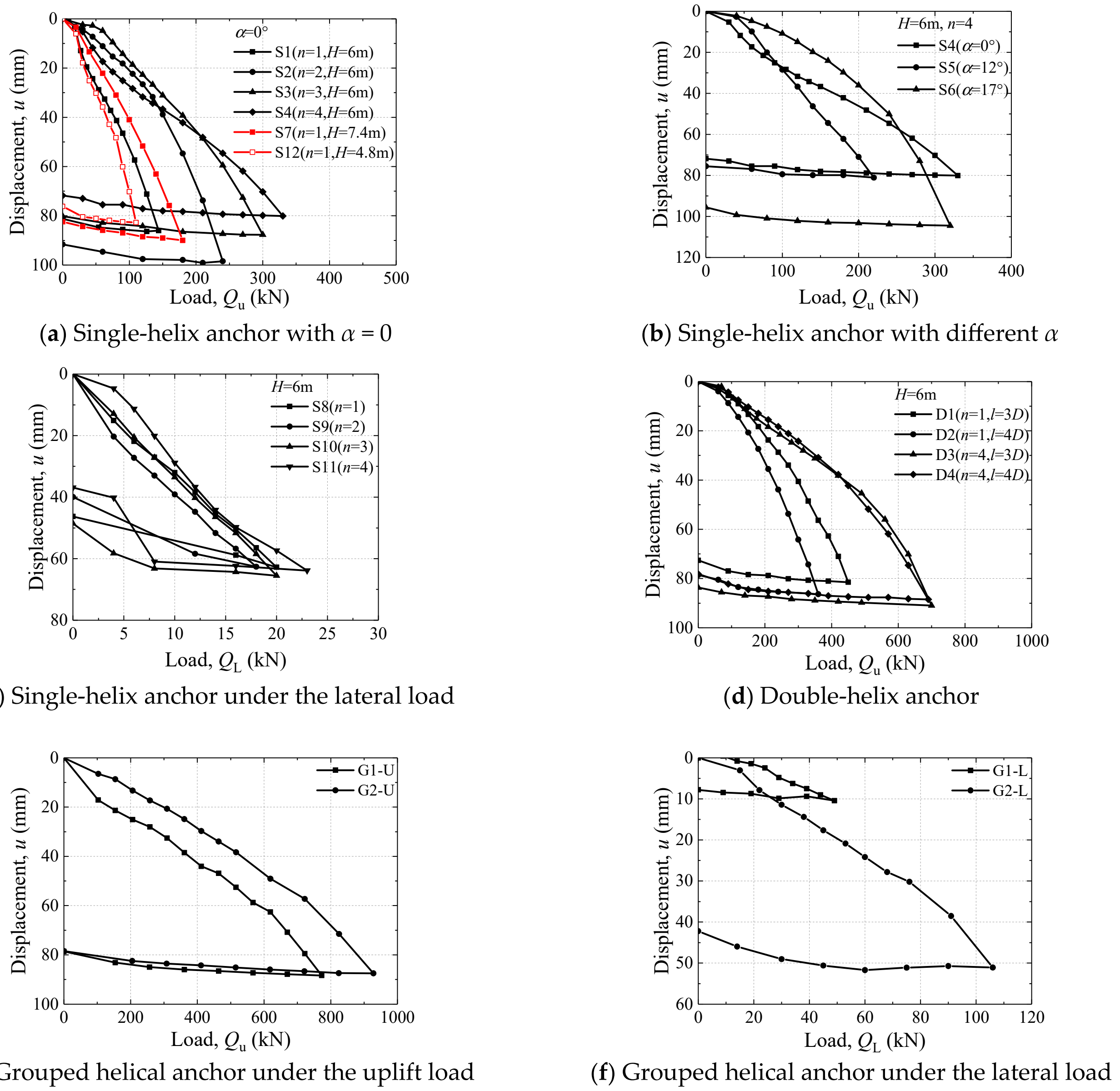

(**a**) Single-helix anchor with $\alpha = 0$

(**b**) Single-helix anchor with different α

(**c**) Single-helix anchor under the lateral load

(**d**) Double-helix anchor

(**e**) Grouped helical anchor under the uplift load

(**f**) Grouped helical anchor under the lateral load

Figure 6. The relationship between load and displacement.

It can be found that as the load increases, the displacement increases continuously. During the loading stage under the uplift load, the load–displacement curve of the helical anchor can be divided into three stages, namely the initial straight-line segment, the intermediate curve segment, and the later straight-line segment. During the unloading stage, the load–displacement curve exhibits nonlinear characteristics. Due to the compression of the soil surrounding the anchor plate caused by the load, the stiffness of the soil surrounding the anchor increases, so the slope of the load–displacement curve in the loading stage is smaller than that in the unloading stage. That is to say, the initial elastic modulus of the soil is smaller than the rebound modulus of the soil. During the loading stage under lateral load, the load–displacement curve of the helical anchor is basically linear. During the unloading stage under lateral load, the load–displacement curve also exhibits nonlinear characteristics. For the same reason as above, the initial elastic modulus of soil under lateral load is also smaller than the rebound modulus of soil.

There are several methods that can be used to evaluate the uplift failure capacity of helical anchors such as the Brinch–Hansen criterion, Davisson criterion, Federal Highway Administration FHWA (5% of the helix diameter), L1–L2 method, and ISSMFE (10% of the helix diameter). The ISSMFE deals with finding the load at a displacement value of the helix plate diameter [8,36–38]. Many researchers have unanimously agreed that the failure of helical anchors can occur at the displacement of 10%D [33]. However, research on the failure capacity of helical anchors under lateral loads is limited. The selection of failure criteria will lead to different bearing capacities, further affecting the study of group anchoring effects. In this study, different failure criteria were used to determine the failure capacity of the helical anchor, including the 5%D, 10%D, and 20%D displacement criteria. To standardize the results, the uplift and lateral capacities were normalized. The uplift capacity factor (N_c) was calculated by Equation (3),

$$N_c = \frac{Q_u}{\gamma AH} \tag{3}$$

where Q_u is the uplift failure capacity and γ is the soil effective weight.

Due to the linearity of the load–displacement curve under lateral load, the lateral bearing capacity of helical anchors can be directly calculated by the lateral slope k_L and displacement u_L, and the lateral bearing capacity coefficient can be calculated by Equation (4).

$$N_L = \frac{Q_L}{\gamma AH} = \frac{k_L u_L}{\gamma AH} \tag{4}$$

where Q_L is the lateral failure capacity.

A summary of the different calculated uplift capacity factors, namely $N_{c\text{-}5\%}$, $N_{c\text{-}10\%}$, $N_{c\text{-}20\%}$, and lateral slope k_L, is shown in Table 3.

Table 3. Uplift capacity factor and lateral slope.

Test Number	$N_{c\text{-}5\%}$	$N_{c\text{-}10\%}$	$N_{c\text{-}20\%}$	Test Number	k_L
S1	3.33	7.04	12.29	S8	0.27
S2	8.63	13.71	19.51	S9	0.20
S3	8.63	16.40	25.47	S10	0.31
S4	6.28	15.11	29.64	S11	0.55
S5	7.20	11.38	19.44	G1-H	4.85
S6	12.62	18.96	25.91	G2-H	2.57
S7	3.96	7.25	12.07		
S12	3.72	7.46	12.17		
D1	16.94	26.43	39.89		
D2	13.30	20.21	30.89		
D3	20.35	39.17	59.34		
D4	23.26	38.77	58.37		
G1-U	12.29	47.72	64.99		
G2-U	26.87	33.45	78.84		

4. Discussion

The site test was designed to study the bearing capacity of deep large-sized anchors considering four key variables: embedment depth, plate number, inclination angle, and group effect. The results in Table 3 are used to evaluate each of these variables.

4.1. *Effect of the Embedment Depth and Plate Number*

Figure 7a shows the relationship between the embedment depth ratio (H/D) and the uplift capacity factor of a single-helix-plate anchor, where the embedment depth ratio is the ratio of the embedment depth of the anchor plate to the diameter of the anchor plate.

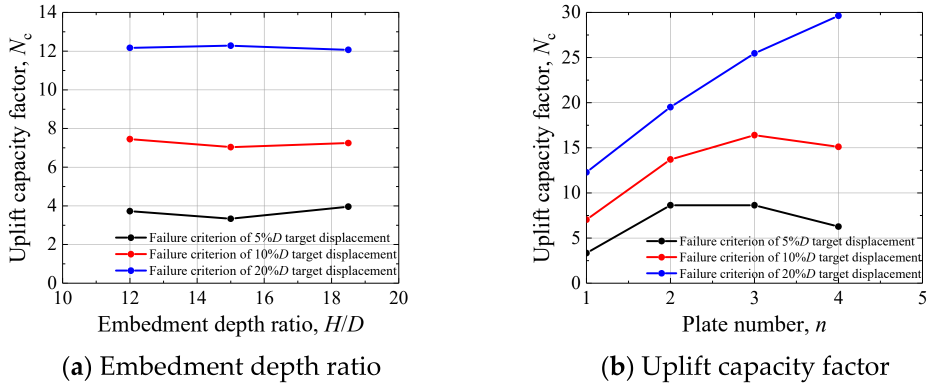

Figure 7. The relationship between the embedment depth ratio and the uplift capacity factor.

It can be observed that the uplift capacity factor is basically constant as the H/D increases. The results show that the influence of the failure criterion on the uplift capacity factor at different embedment depths is mainly reflected in the magnitude of the value, with little effect on the trend in the curve. In addition, this trend in the curve indicates that the helical anchor at this embedment depth is a deep helical anchor.

Figure 7b shows the capacity factors of helical anchors with different numbers of anchor plates but the same embedment depth. It can be seen from Figure 7b that the uplift capacity factor does not increase continuously with the increase in the number of anchor plates adopted with the 5%*D* or 10%*D* failure criterion. This is because when the number of anchor plates exceeds three, due to the shallow embedment depth of the top anchor plate, the overall structure is more likely to be damaged, and the uplift capacity factor is degraded instead. However, the curve trend of the 20%*D* failure criterion is different from that of the 5%*D* and 10%*D* failure criteria. In the S4 test, the uplift capacity is higher than that of other tests. This may be because for the helical anchor with a shallow embedment depth of the top anchor plate, local shear failure occurred, and a small increase in load led to a large displacement.

It can be seen from Table 3 that under lateral load, the lateral slope k_L remains basically unchanged. The lateral capacity of a helical anchor includes the lateral resistance of the anchor shaft, the resistance of the upper and lower deflection edges of the helical plate, and the frictional resistance on the surface of the anchor plate. As the number of anchor plates increases, the resistance of the upper and lower deflection edges of the helical plate increases. There should be an increase in the lateral capacity that is provided. However, the lateral capacity of helical anchors with varying numbers of anchor plates was essentially the same in this field test. The lateral load is not transmitted to the anchor plate, so increasing the number of anchor plates will not significantly improve the lateral capacity. Since the load is only transmitted to the shaft, the lateral slope k_L can be used to characterize the stiffness of the soil.

Comparing Figure 7a,b, it is found that for every 1*D* increase in embedment depth, the uplift capacity increases by 5 kN. For each additional anchor plate, the uplift capacity increases by 74 kN, 30 kN, and −14 kN, respectively. The uplift capacity can be enhanced by increasing the embedment depth; it is not always enhanced by increasing the number of anchor plates. However, a longer shaft will result in a higher slenderness ratio. The shaft's thickness and diameter must be increased in the design, and the capacity of construction equipment must be increased during construction.

Therefore, it is essential to consider the design embedment depth and the number of anchor plates during the design stage. As a deep foundation, it is advisable that helical anchors should be buried as deep as possible according to soil conditions. On this basis, adding appropriate anchor plates can provide higher uplift capacity. It is important to give the top anchor plate's embedment depth more consideration. When the design's lateral load increases, it is advisable to change the geometrical shape of the shaft.

4.2. Effect of the Inclination Angle

Figure 8 shows the uplift capacity factors of single-helix anchors with three different inclination angles with a shaft of the same length. Interestingly, the increase in inclination angle may lead to an increase or decrease in the uplift capacity factor. This may be because the increase in different inclination angles will lead to changes in the embedment depth of the bottom and top anchor plates with the same length shaft. The disturbance area surrounding the anchor plate during installation is also different. If the length of the anchor is increased and the same embedment depth is adopted, the results may be more regular. Therefore, due to limited experimental data, the influence of the inclination angle needs further research.

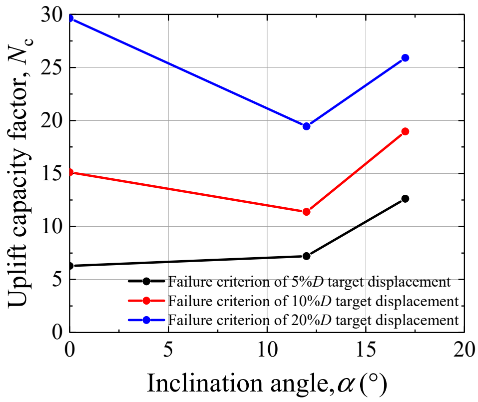

Figure 8. The relationship between the inclination angle and the uplift capacity factor.

4.3. Group Effect

Consistent with conventional deep foundations, one approach to quantifying group effects on uplift capacity is through finding the group efficiency, which is defined by the following equation [21]:

$$\eta = \frac{Q_u}{\sum q_i} \tag{5}$$

where η is group efficiency, Q_u is the capacity of a grouped helical anchor, and $\sum q_i$ is the sum capacity of the single-helix anchor corresponding to the grouped helical anchor.

The group efficiencies of double-helix anchors and grouped helical anchors are calculated as shown in Figure 9. When determining the group efficiency of the G1-U, roughly four S4 tests were used for the calculation.

It can be found from Figure 9 that the group efficiency of double-helix anchors is greater than 1. This phenomenon is also mentioned by Lutenegger [30]. This indicates that there is an interaction between single-helix anchors with a spacing of 3D or 4D. This phenomenon may be related to soil conditions. Compared with two single-helix anchors, the soil between the double-helix anchors is more mobilized, resulting in an increase in bearing capacity. Moreover, as the spacing increases, the group efficiency of the double-helix anchors decreases. That is to say, the mobilized soil decreases with increasing distance. This phenomenon deserves further study. In addition, it can be found that with the increase in failure displacement, the efficiency of group anchors continues to decrease.

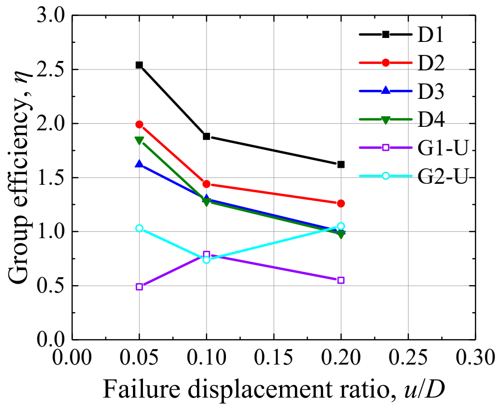

Figure 9. The relationship between the failure displacement and the group efficiency.

From Figure 9, it can be found that the group efficiency of the grouped helical anchor adopted by the G1 configuration does not exceed 1, especially when using the 5%*D* failure criterion, where the group efficiency is only 0.49. However, using the 5%*D* and 20%*D* failure criterion, the efficiency of the grouped helical anchor adopted by the G2 configuration exceeds 1. In addition, the group efficiencies of G1-L and G2-L are 2.19 and 1.54, respectively, indicating that both configurations can improve lateral bearing capacity. Therefore, the G2 configuration of the grouped helical anchor is more highly recommended for this design.

5. Conclusions

This field experiment investigated the performance of helical anchors in clay in terms of uplift and lateral load. The study included 12 single-helix anchors, 4 double-helix anchors, and 4 grouped helical anchors (in two different configurations). The field technique is expected to provide a more accurate representation of the overburden stress and installation circumstances that might potentially arise in a full-scale system. This study examined the effects of embedment depth, number of anchor plates, spacing between anchor shafts, choice of failure criterion, and group effect. The following conclusions may be drawn.

The installation torque increases linearly with depth, which can be represented as $T = 0.8042\ (\text{kN}) \times H$. Simply increasing the number of anchor plates in the design of single-helix anchors while keeping the anchor shaft length the same does not result in a higher uplift and lateral bearing capacity. A suitable inclination angle may enhance the uplift bearing capability. In this soil condition, the group efficiency of double-helix anchors is higher than 1, with different failure criteria. As the failure displacement increases, the group efficiency decreases continuously. However, the maximum group efficiency of grouped helical anchors is 1.05 with a 20%*D* failure criterion. The group efficiency values of G1 and G2 under lateral loads are 2.19 and 1.54, respectively. After comparing the group efficiency and economy of G1 and G2 grouped helical anchors, we can recommended using the G2 configuration. Choice of failure criterion is crucial. The failure criterion affects the uplift bearing capacity trend of single-helix anchors with varying anchor plates as well as the group efficiency trend in grouped helical anchors. However, the failure criterion does not affect the uplift capacity trend of single-helix anchors with varying embedment depths and inclination angles.

Author Contributions: Conceptualization, formal analysis, and writing—review and editing, D.H. and C.Y.; investigation and writing—original draft preparation, C.Y.; investigation and data curation, S.D. and M.D. All authors have read and agreed to the published version of the manuscript.

Funding: This research was funded by the National Natural Science Foundation of China (grant number 52078108).

Data Availability Statement: Due to the nature of this research, participants in this study did not agree for their data to be shared publicly, so supporting data are not available.

Conflicts of Interest: Authors Shijun Ding and Mintao Ding were employed by the company China Electric Power Research Institute. The remaining authors declare that the research was conducted in the absence of any commercial or financial relationships that could be construed as a potential conflict of interest.

References

1. Livneh, B.; El Naggar, M.H. Axial testing and numerical modeling of square shaft helical piles under compressive and tensile loading. *Can. Geotech. J.* **2008**, *45*, 1142–1155. [CrossRef]
2. Merifield, R. Ultimate uplift capacity of multiplate helical type anchors in clay. *J. Geotech. Geoenviron. Eng.* **2011**, *137*, 704–716. [CrossRef]
3. Wang, D.; Merifield, R.; Gaudin, C. Uplift behaviour of helical anchors in clay. *Can. Geotech. J.* **2013**, *50*, 575–584. [CrossRef]
4. Stanier, S.A.; Black, J.A.; Hird, C.C. Modelling helical screw piles in soft clay and design implications. *Proc. Inst. Civ. Eng. Geotech. Eng.* **2014**, *167*, 447–460. [CrossRef]
5. Wang, L.; Wu, M.; Chen, H.; Hao, D.; Tian, Y.; Qi, C. Efficient Machine Learning Models for the Uplift Behavior of Helical Anchors in Dense Sand for Wind Energy Harvesting. *Appl. Sci.* **2022**, *12*, 10397. [CrossRef]
6. Ghaly, A.; Hanna, A.; Hanna, M. Uplift behavior of screw anchors in sand. I: Dry sand. *J. Geotech. Eng.* **1991**, *117*, 773–793. [CrossRef]
7. Drescher, A.; Detournay, E. Limit load in translational failure mechanisms for associative and non-associative materials. *Géotechnique* **1993**, *43*, 443–456. [CrossRef]
8. Hsu, S.; Liao, H. Uplift behaviour of cylindrical anchors in sand. *Can. Geotech. J.* **1998**, *35*, 70–80. [CrossRef]
9. Tappenden, K.M.; Sego, D.C. Predicting the axial capacity of screw piles installed in Canadian soils. In Proceedings of the Canadian Geotechnical Society (CGS), OttawaGeo2007 Conference, Ottawa, ON, Canada, 21–24 October 2007; pp. 1608–1615.
10. White, D.; Cheuk, C.; Bolton, M. The uplift resistance of pipes and plate anchors buried in sand. *Géotechnique* **2008**, *58*, 771–779. [CrossRef]
11. Newgard, J.; Schneider, J.; Thompson, D. Cyclic response of shallow helical anchors in a medium dense sand. In Proceedings of the Frontiers in Offshore Geotechnics III: Proceedings of the 3rd International Symposium on Frontiers in Offshore Geotechnics (ISFOG 2015), Oslo, Norway, 10–12 June 2015; Taylor & Francis Books Ltd.: London, UK, 2015; pp. 913–918.
12. Cerfontaine, B.; Knappett, J.A.; Brown, M.J.; Bradshaw, A.S. Effect of soil deformability on the failure mechanism of shallow plate or screw anchors in sand. *Comput. Geotech.* **2019**, *109*, 34–45. [CrossRef]
13. Tsuha, C.d.H.C.; Aoki, N.; Rault, G.; Thorel, L.; Garnier, J. Physical modelling of helical pile anchors. *Int. J. Phys. Model. Geotech.* **2007**, *7*, 01–12.
14. Hao, D.; Wang, D.; O'Loughlin, C.D.; Gaudin, C. Tensile monotonic capacity of helical anchors in sand: Interaction between helices. *Can. Geotech. J.* **2019**, *56*, 1534–1543. [CrossRef]
15. Al Hakeem, N.; Aubeny, C. Numerical investigation of uplift behavior of circular plate anchors in uniform sand. *J. Geotech. Geoenviron. Eng.* **2019**, *145*, 04019039. [CrossRef]
16. Giampa, J.R.; Bradshaw, A.S.; Schneider, J.A. Influence of dilation angle on drained shallow circular anchor uplift capacity. *Int. J. Geomech.* **2017**, *17*, 04016056. [CrossRef]
17. Spagnoli, G.; de Hollanda Cavalcanti Tsuha, C. A review on the behavior of helical piles as a potential offshore foundation system. *Mar. Georesources Geotechnol.* **2020**, *38*, 1013–1036. [CrossRef]
18. Abdelghany, Y.; El Naggar, M.H. Monotonic and Cyclic Behavior of Helical SCREW Piles under Axial and Lateral Loading. Ph.D. Thesis, The University of Western Ontario, London, ON, Canada, 2010.
19. Davidson, C.; Brown, M.J.; Cerfontaine, B.; Al-Baghdadi, T.; Knappett, J.; Brennan, A.; Augarde, C.; Coombs, W.; Wang, L.; Blake, A. Physical modelling to demonstrate the feasibility of screw piles for offshore jacket-supported wind energy structures. *Géotechnique* **2022**, *72*, 108–126. [CrossRef]
20. Cerfontaine, B.; Knappett, J.; Brown, M.J.; Davidson, C.; Sharif, Y. Optimised design of screw anchors in tension in sand for renewable energy applications. *Ocean Eng.* **2020**, *217*, 108010. [CrossRef]
21. Vignesh, V.; Muthukumar, M. Experimental and numerical study of group effect on the behavior of helical piles in soft clays under uplift and lateral loading. *Ocean Eng.* **2023**, *268*, 113500. [CrossRef]
22. Zhang, R.; Meng, R.; Sang, J.; Hu, Y.; Li, X.; Zheng, C. Modelling individual head-related transfer function (HRTF) based on anthropometric parameters and generic HRTF amplitudes. *CAAI Trans. Intell. Technol.* **2023**, *8*, 364–378. [CrossRef]
23. Luo, C. KELL: A Kernel-Embedded Local Learning for Data-Intensive Modeling. *Artif. Intell. Appl.* **2024**, *2*, 38–44. [CrossRef]
24. Zhang, Y.; Hu, Y.; Gao, X.; Gong, D.; Guo, Y.; Gao, K.; Zhang, W. An embedded vertical-federated feature selection algorithm based on particle swarm optimisation. *CAAI Trans. Intell. Technol.* **2023**, *8*, 734–754. [CrossRef]
25. Simani, S.; Lam, Y.P.; Farsoni, S.; Castaldi, P. Dynamic Neural Network Architecture Design for Predicting Remaining Useful Life of Dynamic Processes. *J. Data Sci. Intell. Syst.* **2023**. [CrossRef]
26. Khan, J.; Lee, E.; Kim, K. A higher prediction accuracy–based alpha–beta filter algorithm using the feedforward artificial neural network. *CAAI Trans. Intell. Technol.* **2023**, *8*, 1124–1139. [CrossRef]
27. Toma, S.; Seto, K.; Chen, W.F. Comparisons of Static and Dynamic Analyses on Toppling Behaviors of Pile Driving Machinery, etc., on Soft Foundation. *Arch. Adv. Eng. Sci.* **2023**, 1–15. [CrossRef]

28. Ghaly, A.; Hanna, A. Model investigation of the performance of single anchors and groups of anchors. *Can. Geotech. J.* **1994**, *31*, 273–284. [CrossRef]
29. Mittal, S.; Mukherjee, S. Vertical uplift capacity of a group of helical screw anchors in sand. *Indian Geotech. J.* **2013**, *43*, 238–250. [CrossRef]
30. Mittal, S.; Mukherjee, S. Vertical pullout capacity of a group of helical screw anchors in sand: An empirical approach. *Indian Geotech. J.* **2014**, *44*, 480–488. [CrossRef]
31. Mittal, S.; Mukherjee, S. Behaviour of group of helical screw anchors under compressive loads. *Geotech. Geol. Eng.* **2015**, *33*, 575–592. [CrossRef]
32. Sakr, M.; Nazir, A.; Azzam, W.; Sallam, A. Uplift capacity of group screw piles with grouted shafts in sand. Capacité d'élévation des pieux à visser de groupe avec des arbres cimentés dans le sable. In Proceedings of the 19th International Conference on Soil Mechanics and Geotechnical Engineering, Seoul, Republic of Korea, 17–21 September 2017.
33. Roy, S.; Bhalla, S.K. Role of geotechnical properties of soil on civil engineering structures. *Resour. Environ.* **2017**, *7*, 103–109.
34. Bradshaw, A.S.; Cullen, L.; Miller, Z. Field study of group effects on the pullout capacity of "deep" helical piles in sand. *Can. Geotech. J.* **2022**, *59*, 538–545. [CrossRef]
35. Ghosh, P.; Samal, S. Interaction effect of group of helical anchors in cohesive soil using finite element analysis. *Geotech. Geol. Eng.* **2017**, *35*, 1475–1490. [CrossRef]
36. Albusoda, B.S.; Abbase, H.O. Performance assessment of single and group of helical piles embedded in expansive soil. *Int. J. Geo-Eng.* **2017**, *8*, 25. [CrossRef]
37. Lutenegger, A.J. Axial uplift of square-shaft single-helix helical anchor groups in Clay. *Innov. Geotech. Eng.* **2018**, 403–416. [CrossRef]
38. Lanyi-Bennett, S.A.; Deng, L. Axial load testing of helical pile groups in glaciolacustrine clay. *Can. Geotech. J.* **2019**, *56*, 187–197. [CrossRef]
39. Elsherbiny, Z.H.; El Naggar, M.H. Axial compressive capacity of helical piles from field tests and numerical study. *Can. Geotech. J.* **2013**, *50*, 1191–1203. [CrossRef]
40. Perko, H.A. *Helical Piles: A Practical Guide to Design and Installation*; John Wiley & Sons: Hoboken, NJ, USA, 2009.
41. Radhakrishna, H. *Helix Anchor Tests in Stiff Fissured Clay*; Ontario Hydro Research Division Research Report; Ontario Hydro Research Division: Parkes, Australia, 1975; pp. 75–123.
42. Al-Baghdadi, T.A.; Brown, M.J.; Knappett, J.A.; Al-Defae, A.H. Effects of vertical loading on lateral screw pile performance. *Proc. Inst. Civ. Eng. Geotech. Eng.* **2017**, *170*, 259–272. [CrossRef]
43. Clemence, S.P.; Pepe, F. Measurement of lateral stress around multihelix anchors in sand. *Geotech. Test. J.* **1984**, *7*, 145–152. [CrossRef]
44. Dickin, E.A. Uplift behavior of horizontal anchor plates in sand. *J. Geotech. Eng.* **1988**, *114*, 1300–1317. [CrossRef]
45. Sakr, M. Lateral resistance of high capacity helical piles–case study. In Proceedings of the 63rd Canadian Geotechnical and 6th Canadian Permafrost Conference, Calgary, AB, Canada, 12–15 September 2010; pp. 12–16.
46. Wu, W.; Lu, C.; Chen, L.; Mei, G.; El Naggar, M.H.; Liu, H. Horizontal vibration characteristics of pile groups in unsaturated soil considering coupled pile–pile interaction. *Ocean Eng.* **2023**, *281*, 115000. [CrossRef]
47. Liu, X.; Wu, W.; El Naggar, M.H.; Sun, J.; Tang, L. Theoretical analysis of dynamic performance of concrete-filled steel tube pile under vertical load. *Comput. Geotech.* **2024**, *165*, 105884. [CrossRef]
48. Yang, X.; Wang, C.; Cao, S.; Wang, F.; Wu, W. Lateral Dynamic Response of Helical Pile in Viscoelastic Foundation Considering Shear Deformation. *Appl. Sci.* **2023**, *13*, 12220. [CrossRef]
49. Chen, L.; Yao, Y.; Liu, H.; Liu, X.; Wu, W.; Mei, G.; El Naggar, M.H. Horizontal vibration characteristics of offshore twin–pile foundations. *Ocean Eng.* **2023**, *290*, 116101. [CrossRef]
50. Wu, W.; Zhang, Y. A review of pile foundations in viscoelastic medium: Dynamic analysis and wave propagation modeling. *Energies* **2022**, *15*, 9432. [CrossRef]
51. Kavvadas, M.; Amorosi, A. A constitutive model for structured soils. *Géotechnique* **2000**, *50*, 263–273. [CrossRef]
52. Savvides, A.A.; Papadrakakis, M. A computational study on the uncertainty quantification of failure of clays with a modified Cam-Clay yield criterion. *SN Appl. Sci.* **2021**, *3*, 659. [CrossRef]
53. *ASTM D3689/D3689M-07(2013)e1*; Standard Test Methods for Deep Foundations under Static Axial Tensile Load. ASTM: West Conshohocken, PA, USA, 2013. [CrossRef]
54. Zhang, D.J.Y. Predicting Capacity of Helical Screw Piles in Alberta Soils. Master's Thesis, University of Alberta, Edmonton, AB, Canada, 1999.